Noncompetitive Antagonist Binding Sites in the *Torpedo* Nicotinic Acetylcholine Receptor Ion Channel. Structure−Activity Relationship Studies Using Adamantane Derivatives†

Hugo R. Arias,*,‡ James R. Trudell,§ Erin Z. Bayer,|| Brent Hester,|| Elizabeth A. McCardy,|| and Michael P. Blanton||

Department of Pharmaceutical Sciences, College of Pharmacy, Western University of Health Sciences, Pomona, California 91766-1854, Departments of Pharmacology and Anesthesiology, School of Medicine, Texas Tech University Health Sciences Center, Lubbock, Texas 79430, and Department of Anesthesia, Stanford University School of Medicine, Stanford, California 94305

Received January 13, 2003; Revised Manuscript Received April 30, 2003

ABSTRACT: We used a series of adamantane derivatives to probe the structure of the phencyclidine locus in either the resting or desensitized state of the nicotinic acetylcholine receptor (AChR). Competitive radioligand binding and photolabeling experiments using well-characterized noncompetitive antagonists such as the phencyclidine analogue [*piperidyl*-3,4-^{3}H(N)]-*N*-[1-(2-thienyl)cyclohexyl]-3,4-piperidine ([^{3}H]-TCP), [^{3}H]ethidium, [^{3}H]tetracaine, [^{14}C]amobarbital, and 3-(trifluoromethyl)-3-(*m*-[^{125}I]iodophenyl)-diazirine ([^{125}I]TID) were performed. Thermodynamic and structure−function relationship analyses yielded the following results. (1) There is a good structure−function relationship for adamantane amino derivatives inhibiting [^{3}H]TCP or [^{3}H]tetracaine binding to the resting AChR. (2) Since the same derivatives inhibit neither [^{14}C]amobarbital binding nor [^{125}I]TID photoincorporation, we conclude that these positively charged molecules preferably bind to the TCP locus, perhaps interacting with αGlu^{262} residues at position M2-20. (3) The opposite is true for the neutral molecule adamantane, which prefers the TID (or barbiturate) locus instead of the TCP site. (4) The TID site is smaller and more hydrophobic (it accommodates neutral molecules with a maximal volume of 333 ± 45 Å^3) than the TCP locus, which has room for positively charged molecules with volumes as large as 461 Å^3 (e.g., crystal violet). This supports the concept that the resting ion channel is tapering from the extracellular mouth to the middle portion. (5) Finally, although both the hydrophobic environment and the size of the TCP site are practically the same in both states, there is a more obvious cutoff in the desensitized state than in the resting state, suggesting that the desensitization process constrains the TCP locus. A plausible location of neutral and charged adamantane derivatives is shown in a model of the resting ion channel.

The *Torpedo* nicotinic acetylcholine receptor (AChR)[1] is the archetype of a ligand-gated ion channel superfamily found in the nervous system which includes neuronal-type AChRs, type A and C γ-aminobutyric acid, type 3 5-hydroxytryptamine, and glycine receptors (reviewed in refs *1* and *2*). A series of structurally different compounds called noncompetitive antagonists (NCAs) inhibit AChR functions. To date, several topologically distinct NCA binding sites have been characterized in both resting and desensitized AChR ion channels (reviewed in refs *3*−*5*). Previous photoaffinity labeling experiments using [^{3}H]azidophencyclidine have mapped the high-affinity binding site for the dissociative anesthetic phencyclidine (PCP) on both resting and desensitized AChRs to a proteolytic fragment containing transmembrane segments M1−M3 (*6*). In the desensitized AChR, PCP displaces ethidium from its high-affinity binding site with an inhibition constant [$K_i \sim 0.3$ μM (*7*)] similar to its dissociation constant [$K_d = 0.3-0.8$ μM (*7*−*9*)], suggesting a common location. In turn, a luminal location for the ethidium binding site has been deduced by using photoaffinity labeling (*10*) and fluorescence resonance energy transfer approaches (*11*). More specifically, [^{3}H]ethidium diazide photolabeled both M1 and M2 transmembrane segments of the α subunit, particularly at residues Leu^{251} (e.g., position M2-9) and Ser^{252} (e.g., position M2-10) (*10*).

† This research was supported by National Institutes of Health Grants R29-NS35786 (M.P.B.) and RO1-GM63034 and RO1-AA013378 (J.R.T.).

* To whom correspondence should be addressed: Department of Pharmaceutical Sciences, College of Pharmacy, Western University of Health Sciences, 309 E. Second St., Pomona, CA 91766-1854. Telephone: (909) 469-5424. Fax: (909) 469-5600. E-mail: harias@westernu.edu.

‡ Western University of Health Sciences.

§ Texas Tech University Health Sciences Center.

|| Stanford University School of Medicine.

[1] Abbreviations: AChR, nicotinic acetylcholine receptor; CCh, carbamylcholine; α-BTx, α-bungarotoxin; NCA, noncompetitive antagonist; PCP, phencyclidine [1-(1-phenylcyclohexyl)piperidine]; TCP, 1-(2-thienylcyclohexyl)piperidine; memantine, 3,5-dimethyl-1-adamantanamine; CrV, crystal violet; [^{3}H]TCP, [*piperidyl*-3,4-^{3}H(N)]-*N*-[1-(2-thienyl)cyclohexyl]-3,4-piperidine; [^{125}I]TID, 3-(trifluoromethyl)-3-(*m*-[^{125}I]iodophenyl)diazirine; [^{3}H]H_{12}-HTX, [^{3}H]perhydrohistrionicotoxin; VDB, vesicle dialysis buffer; IC_{50}, competitor concentration that inhibits 50% drug maximal binding to the AChR; EC_{50}, modulator concentration that enhances 50% drug activity (e.g., binding or photoincorporation) on the AChR; K_i, inhibition constant; K_d, dissociation constant; n_H, Hill coefficient; *P*, partition coefficient; $\Delta\Delta G°$, differential free energy change; $\Delta G°$, free energy change.

10.1021/bi034052n CCC: $25.00
Published on Web 00/00/0000 PAGE EST: 12.9

In the resting ion channel, there are at least two allosterically linked NCA binding sites. The first is an overlapping binding site for barbiturates and the hydrophobic probe 3-(trifluoromethyl)-3-(*m*-[^{125}I]iodophenyl)diazirine ([^{125}I]TID) (*12*), which is located approximately in the middle of each channel-lining M2 segment, more specifically between the highly conserved ring of leucine residues (M2-9, e.g., δLeu^{265}) and the ring of valine residues (M2-13, e.g., δVal^{269}) (*13*−*16*). The other site, which is located more extracellularly (above position M2-13 and extending to position M2-20), includes the locus for the dissociative anesthetics ketamine, PCP, and its structural analogue TCP (*17*, *18*). This location is based in part on the results from this paper. The tetracaine binding domain partially overlaps the TID site (M2-9 and M2-13), but includes additional residues at M2-5 (e.g., αIle^{247}) and M2-12 (e.g., δAla^{268}) (*19*). Competitive binding studies along with molecular modeling (*18*) indicate that the tetracaine molecule bridges both the TID (i.e., the barbiturate) and the PCP (i.e., the ketamine) binding site. Another important conclusion is that activation of the receptor which induces the resting → open → desensitized conformation state transitions results in state-dependent changes in the location of NCA sites (e.g., TID) and therefore concomitant changes in the properties of the binding site (e.g., size, hydrophobicity, etc.).

The antiparkinsonian and antiviral drug amantadine (1-adamantanamine), as well as its derivatives, inhibits both muscle-type (*20*−*23*) and neuronal-type AChRs (*24*−*28*) in a noncompetitive manner. However, the inhibitory mechanism for AChRs is not clear. There is evidence indicating an open channel blocking mechanism (*21*, *25*, *27*), but additional experimental results also show that several adamantane derivatives may bind and/or induce either the resting or desensitized receptor state (*21*, *25*), suggesting an allosteric mode of inhibition.

Amantadine displaces the high-affinity NCA perhydrohistrionicotoxin ([^{3}H]H$_{12}$-HTX) from its site within the ion channel (*20*, *21*), and considering the insinuation by Gallagher et al. (*17*) that HTX may bind to the PCP locus, amantadine might bind to the PCP site as well. In this regard, we used the radioligand [^{3}H]TCP as a structural analogue of [^{3}H]PCP (*29*, *30*), and a series of adamantane derivatives to probe the molecular structure of the PCP binding site in both resting and desensitized AChR ion channels. More specifically, we tested the ability of adamantane, azidoadamantane, 1-adamantanamine, 2-adamantanamine, memantine, adamantylethylamine, adamantanemethylamine, and adamantylpyridinium (see molecular structures in Figure 1) to affect the binding of [^{3}H]TCP in either the resting or desensitized state. To complete our studies, we performed competitive radioligand binding and photoaffinity labeling experiments using well-characterized NCAs such as [^{3}H]-tetracaine, [^{14}C]amobarbital, and [^{125}I]TID in the resting state, as well as [^{3}H]ethidium in the desensitized state. Since the K_d and stoichiometry for [^{3}H]TCP binding in the resting state have not been reported yet, we also determined these equilibrium binding properties. Finally, we used structural and thermodynamic correlations to determine the molecular components that are involved in the TCP binding site within either the resting or desensitized ion channel.

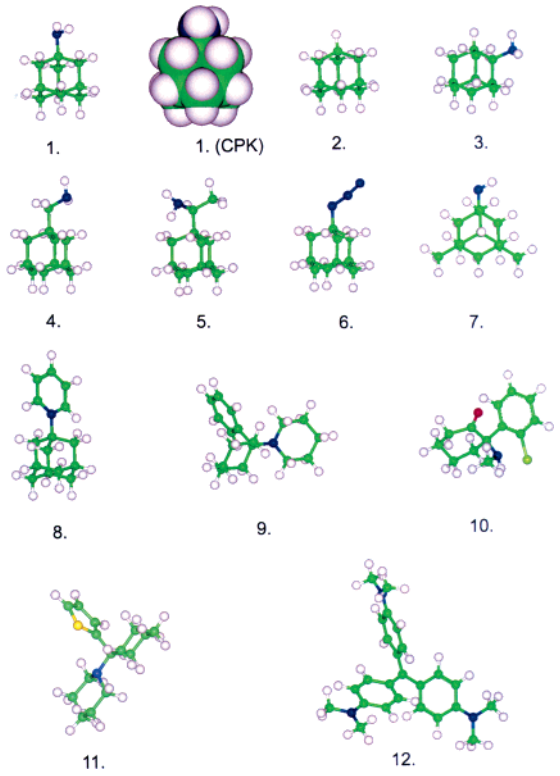

FIGURE 1: Molecular structures of adamantane derivatives and for several dissociative anesthetics. Test molecules were built in Insight 2000 (MSI, San Diego, CA) and are rendered in ball-and-stick format with the exception of 1-adamantanamine which was also rendered with a space-filling surface (CPK) to emphasize the spherical shape. The molecules are (1) 1-adamantanamine, (2) adamantane, (3) 2-adamantanamine, (4) adamantanemethylamine, (5) adamantylethylamine, (6) azidoadamantane, (7) memantine, (8) adamantylpyridinium, (9) phencyclidine, (10) ketamine, (11) TCP, and (12) crystal violet.

EXPERIMENTAL PROCEDURES

Materials. [*piperidyl*-3,4-^{3}H(N)]-*N*-[1-(2-thienyl)cyclohexyl]-3,4-piperidine ([^{3}H]TCP, 41.8−57.6 Ci/mmol) was obtained from New England Nuclear Research Products (Boston, MA) and 3-(trifluoromethyl)-3-(*m*-[^{125}I]iodophenyl)diazirine ([^{125}I]-TID, ∼10 Ci/mmol) from Amersham Pharmacia Biotech (Piscataway, NJ), and both were stored in ethanol at −20 and 4 °C, respectively. [^{3}H]Tetracaine (36 Ci/mmol) and [^{3}H]-ethidium (8.2 Ci/mmol) were a gift from J. Cohen (Harvard Medical School, Boston, MA) and Steen Pedersen (Baylor College of Medicine, Houston, TX), respectively, and both were stored in ethanol at −20 °C. [^{14}C]Amobarbital (50 mCi/mmol) was synthesized by American Radiolabeled Chemicals (St. Louis, MO) and was stored in ethanol at −20 °C. Suberyldicholine dichloride, carbamylcholine chloride, tetracaine hydrochloride, phencyclidine hydrochloride (PCP), thienylcyclohexylpiperidine hydrochloride (TCP), 3,5-dimethyl-1-adamantanamine hydrochloride (memantine), and 1-adamantanamine hydrochloride (amantadine) were purchased from Sigma Chemical Co. (St. Louis, MO). 2-Adamantanamine hydrochloride, 1-azidoadamantane, 1-(1-adamantyl)pyridinium bromide, 1-(1-adamantyl)ethylamine hydrochloride, adamantane, and 1-adamantane methylamine were obtained from Aldrich Chemical Co., Inc. (Milwaukee, WI). [1-(Dimethylamino)naphthalene-5-sulfonamido]ethyltrimethylammonium perchlorate (dansyltrimethylamine) was

obtained from Pierce Chemical Co. (Rockford, IL). Other organic chemicals were of the highest available purity.

Preparation of AChR Native Membranes. AChR native membranes were prepared from frozen *Torpedo californica* electric organs obtained from Aquatic Research Consultants (San Pedro, CA) by differential and sucrose density gradient centrifugation, as described previously (*31*). The specific activities of these membrane preparations were determined by the decrease in dansyltrimethylamine (6.6 μM) fluorescence produced by the titration of suberyldicholine into receptor suspensions (0.3 mg/mL) in the presence of 100 μM PCP and ranged from 0.9 to 1.6 nmol of suberyldicholine binding sites/mg of total protein (0.45−0.80 nmol of AChR/mg of protein). Dansyltrimethylamine excitation and emission wavelengths were 280 and 546 nm, respectively. To reduce stray-light effects, a 530 nm cutoff filter was placed in the path of the dansyltrimethylamine emission beam. The AChR membrane preparations (in ~36% sucrose and 0.02% NaN_3) were stored at −80 °C.

Equilibrium Binding of [^{3}H]TCP to AChR in the Resting State. The binding of [^{3}H]TCP to native AChR-rich membranes was assessed with a centrifugation assay similar to that described for [^{3}H]PCP binding (*7*). Briefly, AChR membranes (0.3 μM AChR) were suspended in vesicle dialysis buffer (VDB) [10 mM MOPS, 100 mM NaCl, 0.1 mM EDTA, and 0.02% NaN_3 (pH 7.5)] with increasing concentrations of [^{3}H]TCP, in the absence of carbamylcholine (CCh) or in the presence of 1 μM α-bungarotoxin (α-BTx), a ligand which stabilizes the AChR in the resting state (*32*). The [^{3}H]TCP/TCP concentration ratio was less than 0.005; thus, the actual TCP concentration ([^{3}H]TCP + unlabeled TCP) was not significantly different from the unlabeled TCP concentration. The final concentration of TCP ranged between 0.2 and 9 μM. Since previous experiments indicated that tetracaine inhibits [^{3}H]TCP binding to the resting AChR with high affinity [~0.7 μM (*18*)], a parallel set of tubes was prepared containing 100 μM tetracaine to determine the extent of nonspecific [^{3}H]TCP binding. The membrane suspensions were equilibrated for 1 h at room temperature (RT). Bound ([B]) [^{3}H]TCP was then separated from the free ([F]) ligand by centrifugation at 18 000 rpm for 1 h using a JA-20 rotor in a Beckman J2-HS centrifuge (Beckman Coulter, Inc., Fullerton, CA). After centrifugation, 50 μL aliquots of the supernatant were removed and assayed for total radioactivity in 3 mL of Bio-Safe II (Research Products International Corp., Mount Prospect, IL) using a Packard 1900 TR scintillation counter. The remainder of the supernatant was aspirated; the tubes were inverted and allowed to drain for 30 min, and then any residual liquid was removed with a cotton swab. The pellets were resuspended in 100 μL of 10% SDS and transferred to scintillation vials with 3 mL of Bio-Safe II, and the radioactivity (^{3}H disintegrations per minute) was determined.

Using the graphics program Prism (GraphPad), binding data were fit to the Rosenthal−Scatchard plot (*33*) using the equation

$$[B]/[F] = -[B]/K_d + B_{max}/K_d \quad (1)$$

where B_{max}, the number of TCP binding sites, can be estimated from the *x*-intercept (when $y = 0$) of the plot [B]/[F] versus [B]. The number of TCP binding sites per receptor is then calculated from the concentration of AChRs (0.3 μM). The K_d of TCP is obtained from the negative reciprocal of the slope. The standard deviation in the calculated value is also reported.

Effect of Adamantane Derivatives on either [^{3}H]TCP, [^{3}H]-Tetracaine, or [^{14}C]Amobarbital Binding to Resting AChRs. The effect of adamantane, azidoadamantane, 1-adamantanamine, 2-adamantanamine, adamantylpyridinium, adamantylethylamine, adamantanemethylamine, and memantine (see Figure 1 for molecular structures) on [^{3}H]TCP, [^{3}H]tetracaine, or [^{14}C]amobarbital binding to the resting AChR was examined. AChR native membranes were suspended in 8 mL of VDB buffer (0.2 μM AChR) with either 7.5 μM [^{14}C]-amobarbital, 5.9 nM [^{3}H]TCP, or 4.3 nM [^{3}H]tetracaine, in the absence of CCh. To be certain that in the absence of agonist and in the presence of a competing ligand the AChR remains predominantly in the resting state (*32*), we performed several control experiments. First, we examined TCP inhibition of [^{3}H]tetracaine binding both in the absence of agonist and in the presence of 1.5 μM α-BTx, a ligand which stabilizes the AChR in the resting state (*32*). Second, we examined inhibition of [^{3}H]TCP binding by memantine in the absence of agonist and in the presence of 1.5 μM α-BTx.

The total membrane suspension was then divided into aliquots, and increasing concentrations of the drug that was being studied were added (depending on the drug being used, the concentration ranged between 0.01 and 2000 μM). The level of nonspecific binding was determined in the presence of 100−200 μM tetracaine. After centrifugation of the samples (18 000 rpm for 1 h), the ^{14}C- or ^{3}H-containing pellets were resuspended in 100−200 μL of 10% SDS and transferred to a scintillation vial with 3−5 mL of Bio-Safe II. The bound fraction was determined by scintillation counting.

Effect of Adamantane Derivatives on either [^{3}H]TCP or [^{3}H]Ethidium Binding to Desensitized AChRs. For experiments on the inhibition of [^{3}H]TCP binding to desensitized AChRs by adamantane derivatives, the same protocol as in the resting state was used but in the presence of 1 mM CCh to desensitize the AChR, and 100 μM TCP to determine the extent of nonspecific [^{3}H]TCP binding. With regard to the experiments on the inhibition of [^{3}H]ethidium binding to desensitized AChRs by adamantane derivatives, an initial concentration of 0.4 μM [^{3}H]ethidium was used.

Effect of Adamantane Derivatives on [^{125}I]TID Photoincorporation into the Resting AChR. To determine the effect of several adamantane derivatives on [^{125}I]TID photoincorporation into the AChR, 0.2 μM AChR native membranes were suspended in 8 mL of VDB, with ~430 nM [^{125}I]TID, in the absence of CCh (resting state). The total volume was then divided into aliquots, and increasing concentrations of adamantane, memantine, and 1- and 2-adamantanamine (from 1 to 120 μM) were added from ethanolic stock solutions (ethanol concentration of <1%) to each tube. The membrane suspension was allowed to incubate for 1 h at room temperature. Membranes were then irradiated for 7 min at a distance of <1 cm with a 365 nm lamp (Spectroline model EN-280L; Spectronics, Westbury, NY) and labeled polypeptides separated by SDS−PAGE (*34*). After electrophoresis, the polypeptides in the polyacrylamide gel were visualized with Coomassie blue stain, and following autoradiographic analysis of the dried gel (*34*), the gel band for each AChR

Table 1: Effect of Adamantane Derivatives on Binding of [^{3}H]TCP, [^{3}H]Tetracaine, and [^{14}C]Amobarbital to and Photoincorporation of [^{125}I]TID into the Resting AChR

	[^{3}H]TCP		[^{3}H]tetracaine		[^{14}C]amobarbital		[^{125}I]TID	
adamantane derivative	K_i (μM)	n_H[b]	K_i (μM)	n_H[b]	EC_{50} (μM)	n_H[b]	EC_{50} (μM)	n_H[b]
memantine	3.0 ± 0.2	0.96 ± 0.06	3.3 ± 0.3	0.96 ± 0.06	1.7 ± 1.3	0.63 ± 0.57	3.1 ± 0.9	1.50 ± 0.56
adamantylethylamine	10.0 ± 1.0	0.93 ± 0.07	6.1 ± 0.5	1.21 ± 0.12	no effect	–	–	–
1-adamantanamine	19.0 ± 1.5	0.90 ± 0.06	15.8 ± 1.8	1.06 ± 0.11	1.2 ± 0.5	1.14 ± 0.48	12.7 ± 3.3	0.80 ± 0.16
2-adamantanamine	29.8 ± 3.7	0.96 ± 0.07	17.3 ± 4.4	0.95 ± 0.20	4.4 ± 1.5	1.89 ± 0.58	79.3 ± 26.0	0.50 ± 0.11
adamantanemethylamine	47.3 ± 3.6	0.91 ± 0.06	25.6 ± 3.2	1.12 ± 0.14	no effect	–	–	–
adamantylpyridinium	186 ± 17	1.03 ± 0.10	208 ± 28	1.10 ± 0.15	no effect	–	–	–
azidoadamantane	208 ± 104	0.94 ± 0.64	68.4 ± 14.6	0.90 ± 0.18	~22 000[c]	0.21 ± 0.08	–	–
adamantane	20.5 ± 12.2[a]	0.85 ± 0.61	143 ± 30	0.91 ± 0.18	102 ± 25	1.40 ± 0.44	79.6 ± 6.1[c]	0.89 ± 0.07

[a] This is an EC_{50} value. [b] Hill coefficients. [c] These are K_i values.

Table 2: Effect of Adamantane Derivatives on Binding of either [^{3}H]TCP or [^{3}H]Ethidium to the Desensitized AChR

	[^{3}H]TCP		[^{3}H]ethidium	
adamantane derivative	K_i (μM)	n_H[a]	K_i (μM)	n_H[a]
memantine	5.5 ± 1.6	1.00 ± 0.27	8.6 ± 3.0	0.82 ± 0.16
adamantylethylamine	8.5 ± 0.7	0.98 ± 0.07	15.9 ± 4.1	0.83 ± 0.13
1-adamantanamine	72.6 ± 12.2	1.09 ± 0.21	42.1 ± 8.7	0.92 ± 0.12
2-adamantanamine	106 ± 19	0.92 ± 0.17	66.7 ± 17.2	0.92 ± 0.17
adamantanemethylamine	37.7 ± 4.1	1.04 ± 0.11	54.3 ± 11.7	0.85 ± 0.11
adamantylpyridinium	93.7 ± 5.0	1.01 ± 0.05	–	–
azidoadamantane	~755	0.81 ± 0.52	–	–
adamantane	~76 000	0.32 ± 0.22	no effect	–

[a] Hill coefficients.

subunit was excised and the amount of ^{125}I counts per minute measured with a Packard Cobra II γ-counter. Nonspecific photoincorporation was assessed in the presence of 400 μM CCh as described previously (*34*). The level of specific photoincorporation in each subunit (α, β, γ, and δ) was averaged.

Data Analysis. For the binding and photoincorporation experiments described above, the concentration−response data were curve-fitted by nonlinear least-squares analysis using Prism (GraphPad) and the corresponding EC_{50} (potentiation) and IC_{50} (inhibition) values calculated. The EC_{50} values as well as the n_H values are summarized in Table 1. If the fact that the AChR presents one binding site for TCP in either the resting (this paper) or desensitized state (*29*, *30*) is taken into account, as well as a single high-affinity locus for ethidium (*7*, *11*), tetracaine (*13*), amobarbital (*12*), and TID (*15*) in the resting state, the observed IC_{50} values from the competition experiments were transformed into K_i values using the Cheng−Prusoff relationship (*35*):

$$K_i = IC_{50}/(1 + [NCA]/K_d^{NCA}) \quad (2)$$

where [NCA] is the initial concentration of the labeled NCA ([^{3}H]TCP, [^{3}H]tetracaine, [^{14}C]amobarbital, or [^{125}I]TID) and K_d^{NCA} is the dissociation constant for TCP [0.83 μM in the resting state (this paper) and 0.25 μM in the desensitized state (*30*)], ethidium [1.6 μM (*7*)], tetracaine [0.5 μM (*13*)], amobarbital [3.7 μM (*12*)], and TID [4 μM (*15*)]. The calculated K_is and Hill coefficients (n_Hs) are summarized in Tables 1 and 2, respectively.

Determination of the Differential Free Energy Change by the Addition or Change in the Position of Distinct Chemical Groups on the Adamantane Molecule. The free energy change ($\Delta G°$) of equilibrium binding of a molecule to its receptor can be thermodynamically defined by the following equation (for a review, see ref *4*):

$$\Delta G° = RT \ln(K_d \text{ or } K_i) \quad (3)$$

where R is the universal gas constant (8.314 J mol^{-1} K^{-1}) and T is the absolute temperature in kelvin. Within the same concept, the differential free energy change ($\Delta\Delta G°$), determined by the equilibrium binding properties of one molecule *a* in comparison to another structurally distinct molecule *b*, can be defined as (for a review, see ref *4*):

$$\Delta G°a - \Delta G°b\ (\Delta\Delta G°) = RT \ln(K_i a/K_i b) \quad (4)$$

where $K_i a$ and $K_i b$ are the inhibition constants for compounds *a* and *b*, respectively. The use of this equation give us details about the chemical determinants of the drug that are involved in the process of binding to its receptor locus. For instance, we used this relationship to determine the effect of the addition of an amino (i.e., 1-adamantanamine) or an azido group (i.e., azidoadamantane) to the adamantane molecule (e.g., $\Delta G°$*adamantane* − $\Delta G°$*1-adamantanamine* or $\Delta G°$ *adamantane* − $\Delta G°$*azidoadamantane*, respectively), the addition of two methyl groups to the 1-adamantanamine molecule to obtain memantine, the addition of either a methylene (e.g., adamantanemethylamine) or alkyl (e.g., adamantylethylamine) group to the 1-adamantanamine molecule, and the position of the ammonium group in adamantanamine isomers. The calculated $\Delta\Delta G°$ values were summarized in Table 3. Negative $\Delta\Delta G°$ values indicate that the observed structural change (e.g., addition of a chemical group, greater distance between the adamantane ring and the amino group, etc.) results in a higher affinity at the AChR, whereas positive values indicate that the observed structural change results in a lower affinity at the AChR.

Table 3: Differential Free Energy Change ($\Delta\Delta G°$)[a] for the Addition or Distinct Position of Specific Chemical Groups on the Adamantane Molecule in either the Resting or Desensitized State

		$\Delta\Delta G°$ (kJ/mol)			
		resting state		desensitized state	
chemical group	structural comparison	tetracaine experiments	TCP experiments	TCP experiments	ethidium experiments
ammonium (H_3N^+)	adamantane vs 1-adamantanamine	-5.5 ± 0.5	–	-17.2 ± 0.4	–
azido (N_3)	adamantane vs azidoadamantane	-1.8 ± 0.7	–	–	–
position of H_3N^+	1- vs 2-adamantanamine	~0.2	1.1 ± 0.3	0.9 ± 0.5	1.1 ± 0.7
methyl (two CH_3 groups)	1-adamantanamine vs memantine	-3.9 ± 0.3	-4.6 ± 0.2	-6.4 ± 0.7	-4.9 ± 0.9
methylene (CH_2)	1-adamantanamine vs adamantanemethylamine	1.6 ± 0.4	2.3 ± 0.2	-1.6 ± 0.4	0.6 ± 0.6
alkyl chain (=$CHCH_3$)	1-adamantanamine vs adamantylethylamine	-2.6 ± 0.3	-1.6 ± 0.3	-5.3 ± 0.4	-2.4 ± 0.7

[a] The $\Delta\Delta G°$ values were calculated according to eq 4 (for a review, see ref *4*). Positive and negative values indicate that the specific structural change reduces and increases drug affinity, respectively.

Hydrophobicity and Molecular Volume of Adamantane Derivatives. The relative hydrophobicity of a drug, as measured by the log of its octanol/water partition coefficient (log *P*), is a good predictor of potency and bioavailability (*36*). We used several methods to estimate log *P* values. One approach was to use programs that are parametrized to add values characteristic of functional groups and atom types. We used the algorithms described by Crippen's (*37*) and Villar's group (*38*, *39*) that are modules in the Spartan program (Wavefunction Inc., San Diego, CA), and a third algorithm available in the Cache program (Fujitsu America, Beaverton, OR). The log *P* values obtained using the Chose−Crippen algorithm found in the Cache program are as follows: 6.16 [crystal violet (CrV)] > 3.98 (PCP) > 3.17 (ketamine) > 3.13 (TCP) > 2.89 (admantylpyridinium) > 2.69 (adamantane) > 2.50 (azidoadamantane) > 2.19 (adamantylethylamine) > 1.97 (memantine) > 1.78 (adamantanemethylamine) > 1.43 (2-adamantanamine) > 1.11 (1-adamantanamine). The fact that 2-adamantanamine has a log *P* value that is greater than that of 1-adamantanamine may be due to the fact that position 1 in the adamantane molecule is a tertiary carbon center at a bridgehead site, whereas position 2 is a secondary carbon with an adjacent hydrogen.

The approximate van der Waals volumes were also calculated using two approaches. One used fixed values for van der Waals radii of atoms and finds the total volume by an algorithm found in the Spartan program that subtracts the overlap between many spheres that make up a molecule (*40*). This technique is robust and self-consistent within a homologous series of molecules. However, it is not sensitive to subtle changes in bonding or electron density. The second technique used the MOPAC semiempirical quantum mechanics program with the AM1 Hamiltonian parameters to calculate the electron density around a molecule and fit a volume envelope (isosurface) to it (*41*). This technique does take into account changes in electron density caused by bonding or altered conformations. However, it is sensitive to the value of electron density (0.002 electron/Å^3) that is chosen to be the limit of the isosurface. Both techniques calculate molecular volumes that are ~30% less than those calculated by dividing the molecular weight by density because they do not take into account vacant space between closely packed molecules. The molecular volume values (in cubic angstroms) obtained using the Spartan program (*40*) are as follows: 461 (CrV) > 311 (PCP) > 302 (TCP) > 267 (ketamine) > 263 (admantylpyridinium) > 233 (adamantylethylamine) > 232 (memantine) > 214 (adamantanemethylamine) > 211 (azidoadamantane) > 192 (1- and 2-adamantanamine) > 177 (adamantane). As expected, both 1- and 2-adamantanamine present the same molecular volume. We used the volumes obtained using this algorithm because they more closely correspond to those calculated for internal cavities in proteins.

Molecular Modeling of the Resting Ion Channel. A model of the five pore-lining helices in the transmembrane domain of *Torpedo* AChR was built by threading five sequences of AChR α1 residues Met^{243}−Glu^{262} onto the backbone of residues Ala^{20}−Ala^{39} from the crystal structure of the bacterial mechanosensitive receptor MscL [PDB entry 1MSL (*42*)]. We used the Homology module of Insight II version 2000.1 (Accelrys, San Diego, CA) (*43*). The MscL pore domain has been suggested to be a progenitor of pentameric ion channels (*42*), and it serves as a good template for a pentameric ion pore. All side chains were adjusted to remove "bumps" with the autorotamer algorithm; the backbone atoms were fixed, and the model was optimized with the Discover module of Insight using a dielectric constant of 4. Then adamantane was added in the center of mass of the pore, and the assembly was re-optimized with no restraints on adamantane. The re-optimization was repeated five times with different starting positions for adamantane, and the ligand returned to essentially the same position each time. Then, memantine was added to this assembly and was manually positioned such that a hydrogen from its amino group formed a hydrogen bond with the carboxylate oxygen of Glu^{262} (at position M2-20). This hydrogen bond was restrained to 2 Å with a 100 kcal/Å^2 tether, and the whole assembly of two ligands and the pore model with the same backbone restrains was optimized, relaxed with 1000 fs of restrained molecular dynamics with 2 fs time steps at 298 K, and then re-optimized to a derivative of 1 kcal/Å with the Discover module.

RESULTS

Equilibrium Binding of [^{3}H]TCP to AChR Membranes in the Resting State. Previous studies demonstrate the presence of a saturatable high-affinity binding site for [^{3}H]TCP on the *Torpedo* AChR when it is in the desensitized state (*29*, *30*). In this paper, we demonstrate that there is also a single high-affinity binding site for [^{3}H]TCP in the resting state. Figure 2 shows the total, nonspecific, and specific [^{3}H]TCP binding to *Torpedo* AChR native membranes in the resting

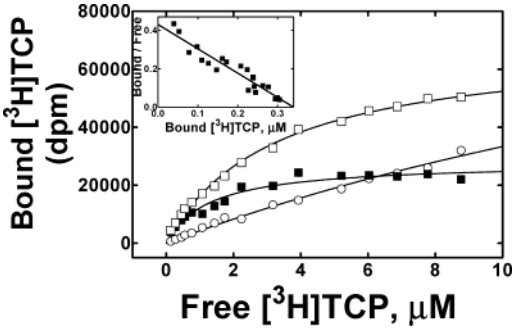

FIGURE 2: [^{3}H]TCP binding to AChR-rich membranes in the resting state. Total (□), nonspecific (○), and specific (■) [^{3}H]TCP binding in the resting state. AChR-rich membranes (0.3 μM) were equilibrated (1 h) with increasing concentrations of [^{3}H]TCP (0.2−9 μM) in the presence of 3 μM α-bungarotoxin. AChR membranes were then centrifuged, and the amount of ^{3}H disintegrations per minute contained in the pellets was measured as described in Experimental Procedures. Nonspecific binding was assessed in the presence of tetracaine (100 μM). Specific or tetracaine-sensitive [^{3}H]TCP binding is defined as total minus nonspecific [^{3}H]TCP binding. The inset shows Rosenthal−Scatchard plots for [^{3}H]TCP specific binding in the resting state. The K_d in the resting state was determined from the negative reciprocal of the slope of three separate experiments according to eq 1, and then averaged. These plots are the result of two different experiments with the standard deviation of the calculated values reported (±).

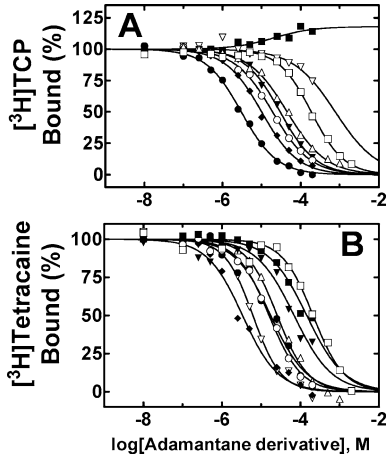

FIGURE 3: Modulation of [^{3}H]TCP (A) and [^{3}H]tetracaine (B) binding to the resting AChR by adamantane derivatives. AChR native membranes (0.2 μM) were equilibrated (1 h) with [^{3}H]TCP (5.9 nM) or [^{3}H]tetracaine (4.2 nM) in the absence of CCh (resting state), and in the presence of increasing concentrations (depending on the used derivative, the concentration ranged between 0.01 and 2000 μM) of adamantane (■), azidoadamantane (▼), adamantylpyridinium (□), adamantanemethylamine (△), 2-adamantanamine (●), 1-adamantanamine (○), adamantylethylamine (▽), and memantine (◆). The AChR membranes were centrifuged, and the radioactivity present in the pellets was measured as described in Experimental Procedures. The level of nonspecific binding was determined in the presence of 100−200 μM tetracaine. Each plot is the average of two different experiments. The concentration-dependent increase in the extent of [^{3}H]TCP binding by adamantane was curve-fitted using a nonlinear least-squares method. The resulting EC_{50} value is summarized in Table 1. The IC_{50} values were determined by a nonlinear least-squares fit for a single binding site. The K_i values were calculated using these IC_{50} values according to eq 2 and are reported in Table 1.

state. The inset of Figure 2 shows the Rosenthal−Scatchard plot for this specific binding. These experimental results indicate the existence of a single (1.10 ± 0.10 binding sites per AChR) high-affinity (K_d = 0.83 ± 0.13 μM) TCP binding site on the *Torpedo* muscle-type AChR. Since equilibrium binding results in the absence of agonist or in the presence of α-BTx are nearly identical, we conclude that the AChR is in the resting state. When the K_d values for [^{3}H]TCP in the desensitized state [0.20−0.25 μM (*29*, *30*)] are taken into account, it is clear that TCP binds with ∼4-fold higher affinity to the desensitized state than to the resting state. These results are similar to that observed for PCP, the structural analogue of TCP, where a ratio of 4.5-fold was observed (*8*).

Inhibition of [^{3}H]TCP and [^{3}H]Tetracaine Binding to the Resting AChR by Adamantane Derivatives. To more fully examine the molecular determinants of the TCP binding site in the resting AChR, we compared the effect of several adamantane derivatives (see molecular structures in Figure 1) on [^{3}H]TCP and [^{3}H]tetracaine binding. In the absence of agonist, memantine, adamantylethylamine, 1-adamantanamine, 2-adamantanamine, adamantanemethylamine, and adamantylpyridinium each completely eliminated specific [^{3}H]TCP and [^{3}H]tetracaine binding to the resting AChR in a concentration-dependent fashion (Figure 3A,B). However, there are interesting differences between both competition experiments. For instance, whereas adamantane does not inhibit (in fact it slightly potentiates) and azidoadamantane slightly inhibits [^{3}H]TCP binding (Figure 3A), both molecules inhibit, albeit with low potency, [^{3}H]tetracaine binding (Figure 3B). In control experiments (data not shown), we determined that TCP inhibits [^{3}H]tetracaine binding to the AChR with nearly identical potency in the absence of agonist (K_i = 2.1 ± 0.3 μM) and in the presence of α-BTx (K_i = 2.5 ± 0.3 μM). In addition, memantine-induced inhibition of [^{3}H]TCP binding in the presence of α-BTx (K_i = 2.8 ± 0.6 μM; data not shown) produced nearly identical results as in the absence of agonist (K_i = 3.0 ± 0.2 μM; see Table 1). These controls demonstrate that memantine inhibits [^{3}H]-TCP binding to the resting AChR. Given the results of these control experiments and since the results of competition binding experiments indicate that each of the other adamantane derivatives binds with equal or greater (apparent) affinity to the resting and desensitized AChR (with n_H values near unity), we conclude that these adamantane derivatives bind to the resting ion channel as well. Nevertheless, we cannot exclude the possibility that these ligands affect a reduction in the level of radioligand binding by inducing a conformational change in the AChR.

From nonlinear least-squares analysis of the binding data, the following rank order of potencies was determined (Table 1): memantine > adamantylethylamine > 1-adamantanamine > 2-adamantanamine > adamantanemethylamine > adamantylpyridinium. The fact that each of these adamantane derivatives completely displaces the binding of either [^{3}H]-TCP or [^{3}H]tetracaine with estimated n_H values near unity suggests that these interactions are formally competitive and are mediated by a mutually exclusive (steric) mechanism. Nevertheless, a strong allosteric mode of inhibition cannot be ruled out.

Potentiation of [^{14}C]Amobarbital Binding and [^{125}I]TID Photoincorporation into the Resting AChR by Adamantane Derivatives. Because the interaction of [^{125}I]TID with the resting AChR has been very well characterized, including identification of a high-affinity binding site within the ion channel pore (*13*, *15*) (reviewed in refs *3*−*5*), we continue

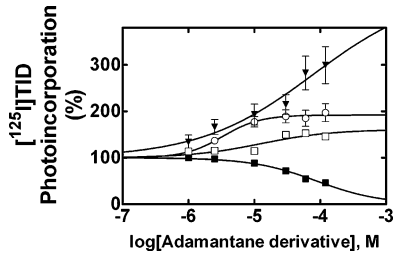

FIGURE 4: Modulation of [^{125}I]TID photoincorporation into AChR subunits in the resting state by adamantane derivatives. AChR native membranes were equilibrated (1 h) with [^{125}I]TID (430 nM) in the presence of increasing concentrations (from 0.1 to 120 μM) of 2-adamantanamine (▼), memantine (○), 1-adamantanamine (□), and adamantane (■). AChR native membranes were then irradiated at 365 nm for 7 min, and polypeptides were resolved by SDS−PAGE. For each concentration of adamantane derivative, individual AChR subunit bands were excised from the dried gel and the amount of [^{125}I]TID photoincorporated into each subunit was determined by γ-counting. Nonspecific binding was assessed in the presence of 400 μM CCh. Each plot is the average of the specific incorporation in each subunit from two different experiments. The concentration-dependent increases in [^{125}I]TID photoincorporation by memantine and 1- and 2-adamantanamine were curve-fitted using a nonlinear least-squares method. The resulting EC_{50} values are summarized in Table 1. The IC_{50} value for adamantane was calculated by a nonlinear least-squares fit for a single binding site. The K_i value was calculated using this IC_{50} according to eq 2 and is reported in Table 1.

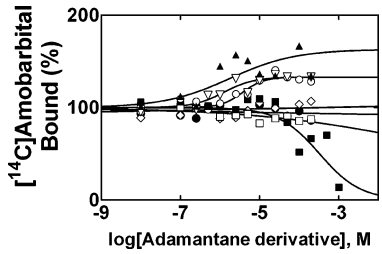

FIGURE 5: Allosteric modulation of [^{14}C]amobarbital binding to the resting AChR by adamantane derivatives. AChR native membranes (0.2 μM) were equilibrated (1 h) with [^{14}C]amobarbital (7.4 μM), in the presence of increasing concentrations (depending on the used derivative, the concentration ranged between 0.01 and 1000 μM) of either adamantane (■), azidoadamantane (□), memantine (▲), adamantanemethylamine (◇), adamantylpyridinium (●), 1-adamantanamine (▽), or 2-adamantanamine (○). AChR native membranes were then centrifuged, and the radioactivity present in the pellet was determined by liquid scintillation counting as described in Experimental Procedures. Nonspecific binding was assessed in the presence of 200 μM tetracaine. Each plot is the average of at least two different experiments. The concentration-dependent increases in [^{14}C]amobarbital binding by memantine and 1- and 2-adamantanamine were curve-fitted using a nonlinear least-squares method, and the resulting EC_{50} values are summarized in Table 1. The IC_{50} values for adamantane and azidoadamantane were calculated by a nonlinear least-squares fit for a single binding site. The K_i values were calculated using these IC_{50}s according to eq 2 and are reported in Table 1.

our studies by examining the effect of several adamantane derivatives on [^{125}I]TID photoincorporation into the resting receptor. AChR native membranes, in the absence of agonist, were equilibrated with ~430 nM [^{125}I]TID and various concentrations of either adamantane, memantine, or the positional isomers 1- and 2-adamantanamine (see molecular structures in Figure 1). Following photolysis, the labeled polypeptides were separated by SDS−PAGE, and the extent of [^{125}I]TID incorporation was assessed by both autoradiography and γ-counting of excised AChR subunit bands. Consistent with previous results (*17*, *34*), [^{125}I]TID was photoincorporated into each AChR subunit, with the γ-subunit labeled ~4-fold greater than each of the other receptor subunits. Somewhat surprisingly, memantine and both adamantanamine positional isomers increased (i.e., potentiated) whereas only adamantane decreased the extent of [^{125}I]TID photoincorporation into each AChR subunit in a concentration-dependent fashion. Figure 4 shows the effect of these adamantane derivatives on [^{125}I]TID photoincorporation into all AChR subunits. The calculated EC_{50} values range from 3 to 80 μM (Table 1). That these adamantane derivatives increase the extent of [^{125}I]TID photoincorporation into the AChR suggests an allosteric mode of interaction (Table 1). Nevertheless, the fact that the n_H value for adamantane is close to unity suggests that this compound might bind, albeit with low affinity, to the TID site in a steric fashion (see Table 1). Although the observed K_i value for adamantane (79.6 ± 6.1 μM) is smaller than that obtained by [^{3}H]-tetracaine competition experiments (143 ± 30 μM), adamantane might bind to the tetracaine domain that is shared with the TID locus.

Because the vast majority (>75%) of [^{125}I]TID photoincorporation into each AChR subunit (labeled in the resting state) reflects incorporation into specific amino acids in the channel-lining M2 segment (*15*, *34*), the presumption is that the potentiation of labeling by adamantane derivatives reflects the increased extent of [^{125}I]TID labeling of the resting ion channel. This conclusion is supported by the fact that potentiation of [^{125}I]TID incorporation into the AChR δ-subunit by PCP or TCP is the result of enhanced labeling of a single residue, δLeu^{265} (i.e., position M2-9) within the δM2 segment (*17*, *18*). A result showing potentiation of [^{125}I]-TID photoincorporation argues strongly for an allosteric interaction between [^{125}I]TID and memantine, or 1- and 2-adamantanamine, and that the binding site for these adamantane derivatives are spatially distinct from the TID binding locus.

We next set out to try to exclude the possibility that the allosteric interaction between either memantine or the two adamantanamine positional isomers and [^{125}I]TID that results in enhanced labeling of the resting channel is somehow an artifact of photolabeling. Because barbiturates and TID bind to the same locus in the resting channel (*12*), we examined the effect of the same derivatives on [^{14}C]amobarbital binding. As shown in Figure 5, memantine and the two positional isomers increase the level of [^{14}C]amobarbital binding to the resting AChR. The calculated EC_{50} values are considerably lower than that obtained by [^{125}I]TID photoincorporation experiments, and range from 1.2 to 4.4 μM (Table 1). That these adamantane derivatives increase the level of [^{14}C]amobarbital binding to the resting AChR suggests an allosteric mode of interaction (Table 1). We also see in Figure 5 that azidoadamantane had virtually no effect on [^{14}C]amobarbital binding to the resting AChR, even at 200 μM, the highest concentration that we tested. Adamantylethylamine (data not shown), adamantanemethylamine, and adamantylpyridinium also did not produce any effect on [^{14}C]amobarbital binding to the resting AChR (Figure 5). On the contrary, adamantane inhibited [^{14}C]amobarbital binding but at concentrations as high as 1 mM (Figure 5). We inferred the K_i values for azidoadamantane and adamantane (Table 1) to compare them with the values obtained by

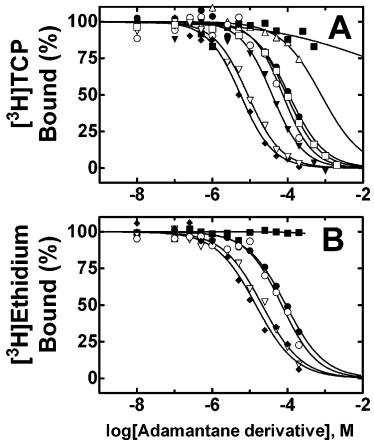

FIGURE 6: Inhibition of [^{3}H]TCP (A) and [^{3}H]ethidium (B) binding to the desensitized AChR by adamantane derivatives. AChR native membranes (0.2 μM) were equilibrated (1 h) with [^{3}H]TCP (5.9 nM) or [^{3}H]ethidium (0.4 μM) in the presence of CCh (desensitized state), and in the presence of increasing concentrations (depending on the used derivative, the concentration ranged between 0.01 and 2000 μM) of adamantane (■), azidoadamantane (△), adamantylpyridinium (□), adamantanemethylamine (▼), 2-adamantanamine (●), 1-adamantanamine (○), adamantylethylamine (▽), and memantine (◆). The AChR membranes were centrifuged, and the radioactivity present in the pellets was measured as described in Experimental Procedures. Nonspecific binding was assessed in the presence of 100−200 μM PCP. Each plot is the average of two different experiments. The IC_{50} values were calculated by a nonlinear least-squares fit for a single binding site. The K_i values were calculated using these IC_{50} values according to eq 2 and are reported in Table 2.

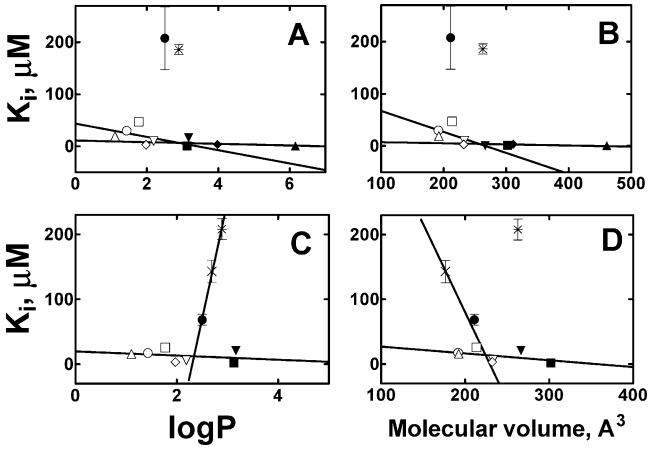

FIGURE 7: Correlation between either the hydrophobicity or molecular volume of each adamantane derivative and its affinity for the TCP (A and B) or tetracaine (C and D) binding site in the resting state. The K_i values for memantine (◇), adamantylethylamine (▽), 1-adamantanamine (△), 2-adamantanamine (○), adamantanemethylamine (□), azidoadamantane (●), adamantylpyridinium (∗), and adamantane (×) were taken from Table 1. We also used the affinity constants for TCP (■), PCP (◆), CrV (▲), and ketamine (▼) to complete our study. (A and C) Hydrophobicity is measured as log *P*, where *P* is the theoretical partition coefficient of each molecule calculated by the Chose−Crippen algorithm found in the Cache program. The intersection point of plot A gives us the minimum log *P* value (2.8 ± 1.0) that is necessary for maximum affinity (lowest K_i values) for the TCP locus. In addition, a maximal log *P* cutoff value of 2.3 ± 0.4 was found in the tetracaine binding site using the data from adamantane, azidoadamantane, and adamantylpyridinium (C). (B and D) Molecular volumes were determined by using the algorithm found in the Spartan program. The intersection point of plot B gives us the minimum molecular volume value (257 ± 64 Å^3) that it is necessary for maximum affinity (lowest K_i values) for the TCP locus. In addition, a minimum molecular volume cutoff value of 224 ± 35 Å^3 was found in the tetracaine binding site using the data from adamantane and azidoadamantane (D).

[^{125}I]TID photoincorporation experiments. Interestingly, the observed K_i for adamantane (102 ± 25 μM) is in the same concentration range as the value obtained by inhibition of [^{125}I]TID photoincorporation (see Table 1). If the fact that both TID and barbiturates bind to overlapping sites (*12*) is taken into account, it is possible that the adamantane locus also overlaps these two sites. On the other hand, whereas azidoadamantane displaces, albeit with low potency, either [^{3}H]tetracaine (Figure 3B) or [^{3}H]TCP binding (Figure 3A), it does not displace [^{3}H]amobarbital binding (Figure 5). This suggests that the azidoadamantane locus is located in another portion of the tetracaine domain that is neither the TCP nor the barbiturate (or the TID) site. One possibility is that its binding site is located near position M2-5 (*19*).

Inhibition of [^{3}H]TCP and [^{3}H]Ethidium Binding to the Desensitized AChR by Adamantane Derivatives. Next, we wished to determine whether the adamantane derivatives bind to the TCP and/or ethidium binding site on the desensitized AChR. To this end, the effect of memantine, adamantylethylamine, 1-adamantanamine, 2-adamantanamine, adamantanemethylamine, adamantylpyridinium, azidoadamantane, and adamantane (see molecular structures in Figure 1) on either [^{3}H]TCP (Figure 6A) or [^{3}H]ethidium (Figure 6B) binding to the AChR in the presence of CCh (desensitized state) was examined. Several adamantane derivatives displaced specific [^{3}H]TCP and [^{3}H]ethidium binding to the desensitized AChR in a concentration-dependent fashion. For example, 200 μM adamantylethylamine inhibited 97% of the specific [^{3}H]TCP binding (Figure 6A). On the other hand, azidoadamantane and adamantane slightly displaced [^{3}H]TCP binding. Nevertheless, we inferred their K_is to compare them with the values obtained in the resting state. In this regard, the rank order of potencies is as follows: memantine > admantylethylamine > adamantanemethylamine > 1-adamantanamine > adamantylpyridinium ∼ 2-adamantanamine ≫ azidoadamantane ≫ adamantane (see Table 2). From these results and considering that the n_H values are close to 1, except for those of adamantane and azidoadamantane (Table 2), we conclude that positively charged adamantane derivatives displace [^{3}H]TCP or [^{3}H]ethidium from its high-affinity binding site in a mutually exclusive (steric) manner when the receptor is in the desensitized state. Although a strong allosteric mode of inhibition cannot be totally ruled out, it is more likely that the locus for these adamantane derivatives, with the exception of azidoadamantane and adamantane, overlaps the TCP or ethidium binding site. Interestingly, both the rank order and the absolute potency of each compound are different relative to that observed in the resting AChR (compare Tables 1 and 2). For example, the observed K_is for 1- and 2-adamantanamine (Table 2) are ∼4-fold higher than those determined in the resting state (Table 1).

Structural Correlation between Hydrophobicity and Molecular Volume of Adamantane Derivatives and Their K_i Values Obtained in either the Resting or Desensitized State. To construct the plots of hydrophobicity (Figure 7A) and molecular volume (Figure 7B) versus K_i values, we used the values for each adamantane derivative obtained from the [^{3}H]-TCP displacement experiments in the resting state (taken

from Table 1), as well as the K_d values for PCP [3.6 ± 0.8 μM (*8*)] and TCP [0.83 ± 0.13 μM (this paper)]. Since ketamine (*18*) and crystal violet (CrV) (*44*) overlap the TCP (or the PCP) binding site in the resting state, we also included their respective affinity values [K_i = 16.5 ± 0.7 μM (*18*), and K_d = 0.63 ± 0.28 μM (*45*)].

The most direct conclusion from these plots is that although the log *P* and molecular volume values for adamantylpyridinium and azidoadamantane are in the same range as those of the other compounds, they do not inhibit [^{3}H]TCP binding with the same potency. This suggests that these two drugs do not bind to the TCP locus. Thus, avoiding the K_i values for azidoadamantane and adamantylpyridinium, we observe a large range of log *P* or molecular volume values where the maximal affinity (lowest K_i values) is practically constant. Nevertheless, a lower affinity is observed at log *P* or molecular volume values of less than ~3 (Figure 7A) or ~250 Å^3 (Figure 7B), respectively. Although there is not a clear-cut correlation, and just for the sake of comparison with the desensitized state, we determined the intersection between the plot formed by the molecules with the highest affinities (e.g., PCP, TCP, CrV, ketamine, memantine, and adamantylethylamine) and the plot corresponding to the other compounds with lower affinities (e.g., adamantanemethylamine and 1- and 2-adamantanamine) as well as memantine and adamantylethylamine. We calculated intersection values of 2.8 ± 1.0 (Figure 7A) and 257 ± 64 Å^3 (Figure 7B), respectively. These values can be considered "minimal cutoff values", which indicate the minimum hydrophobiciy or molecular size that it is necessary for maximal affinity. Nevertheless, molecules with higher log *P* or volume values bind with an even higher affinity. The use of alternative methods to calculate log *P* and molecular volume gives practically the same results (data not shown); log *P* cutoff values of 2.1 ± 0.5 (*38*, *39*), 2.3 ± 0.8 (*37*), and 2.0 ± 0.4 (*41*) as well as a molecular volume cutoff of 275 ± 81 Å^3 (*41*) were calculated.

For the case of the [^{3}H]tetracaine displacement experiments, we constructed the plots of hydrophobicity (Figure 7C) and molecular volume (Figure 7D) versus the K_i values for each adamantane derivative in the resting state (taken from Table 1). Since ketamine and TCP partially overlap the tetracaine binding site in the resting state, we also included their respective K_i values [20.9 ± 3.0 and 2.0 ± 0.4 μM (*18*)]. We observed in these correlations the same details as in the [^{3}H]TCP experiments: (1) adamantylpyridinium is out of any structural correlation, and (2) there is a broad range of log *P* values and molecular volumes that give maximal affinity. Interestingly, we observed a structure−activity relationship for adamantane and azidoadamantane (see Figure 7D), and perhaps adamantylpyridinium (see Figure 7C), which have correlation coefficients (r^2 = 0.88 and 0.82; see panels C and D of Figure 7, respectively) higher than those from [^{3}H]TCP experiments (r^2 = 0.14 and 0.26; see panels A and B of Figure 7, respectively). This suggests that adamantane and azidoadamantane might bind to the portion of the tetracaine domain that does not correspond to the TCP locus. The intersection points give log *P* and molecular volume cutoff values of 2.3 ± 0.4 (see Figure 7C) and 224 ± 35 Å^3 (see Figure 7D), respectively. In this case, and in contrast to the TCP correlation studies, a maximal log *P* value was obtained, indicating that there is a limit for the hydrophobicity of the molecule that allows a maximal affinity. The use of alternative methods to calculate log *P* and the molecular volume gives practically the same results (data not shown); log *P* cutoff values of 1.9 ± 0.3 (*38*, *39*) and 1.6 ± 0.6 (*37*) as well as a molecular volume cutoff of 224 ± 35 Å^3 (*41*) were calculated.

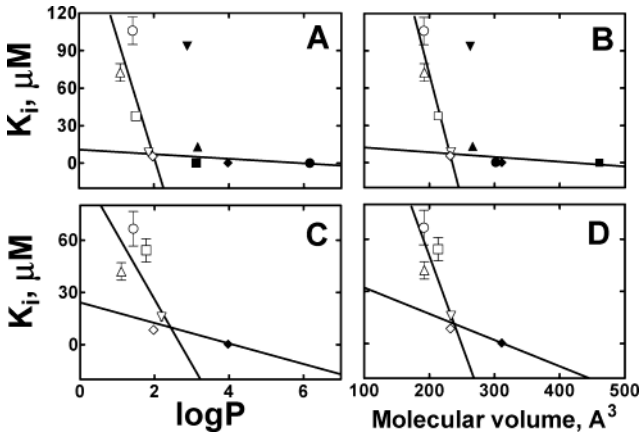

FIGURE 8: Correlation between either (A) the hydrophobicity or (B) molecular volume of each adamantane derivative and its affinity for the TCP (A and B) or ethidium (C and D) binding site in the desensitized state. The K_i values for memantine (◇), adamantylethylamine (▽), adamantanemethylamine (□), 1-adamantanamine (△), 2-adamantanamine (○), and adamantylpyridinium (▼) were taken from Table 2. In addition, we used the affinity constants for TCP (●), PCP (◆), CrV (■), and ketamine (▲). (A and C) Hydrophobicity is measured as log *P*, where *P* is the theoretical partition coefficient calculated by the algorithm found in the Cache program. The intersection point of either plot A or C gives us the minimum log *P* value [2.0 ± 0.4 (A) or 2.4 ± 0.5 (C)] that it is necessary for maximum affinity (lowest K_i values) for the TCP or ethidium locus, respectively. (A and C) Molecular volumes were determined by using the algorithm found in the Spartan program. The intersection point of either panel B or D plots gives us the minimum molecular volume value [232 ± 22 Å^3 (B) or 238 ± 53 Å^3 (D)] that is necessary for maximum affinity for the TCP or ethidium locus, respectively.

For comparative purposes, we also determined the relationship between the IC_{50} values for the TID derivatives used by Blanton et al. (*34*) to study the structure of the TID binding site, and their hydrophobicities or molecular volumes obtained using the same method that was used for adamantane derivatives. From these structure−function relationship studies, maximal cutoff values for log *P* and the molecular volume of 5.6 ± 1.7 and 333 ± 45 Å^3, respectively, were calculated.

With regard to the desensitized state, we constructed the plots of hydrophobicity and molecular volume versus the adamantane derivative K_is obtained from either the [^{3}H]TCP (Figure 8A,B) or [^{3}H]ethidium (Figure 8C,D) displacement experiment (taken from Table 2). We also used the K_d values for PCP [0.30 ± 0.10 μM (*9*)] and TCP [0.25 ± 0.04 μM (*30*)]. Since ketamine (*18*) and CrV (*44*) overlap the TCP (or PCP) binding site in the desensitized state, we also included their corresponding affinity values [K_i = 13.1 ± 1.8 μM (*18*) and K_d = 0.10 ± 0.03 μM (*45*)]. The K_i for PCP [0.3 ± 0.1 μM (*7*)] obtained by inhibition of ethidium binding was also used. For the case of [^{3}H]TCP experiments, a much better correlation between either hydrophobicity [r^2 = 0.60 (Figure 8A)] or molecular volume [r^2 = 0.88 (Figure 8B)] and the K_i values than the correlation found in the experiments in the resting state is depicted. From the

intersection shown in Figure 8A, a minimal log *P* cutoff value of 2.0 ± 0.4 was calculated. This value is practically the same (2.4 ± 0.5) as that calculated using the K_i values from the [^{3}H]ethidium experiment (Figure 8C). From the intersection shown in Figure 8B, a minimal molecular volume cutoff value of 232 ± 22 Å^3 was determined. This value is practically the same (238 ± 53 Å^3) as that calculated using the K_i values from the [^{3}H]ethidium experiment (Figure 8D). The use of alternative methods to calculate log *P* and the molecular volume gives practically the same results for the [^{3}H]TCP experiments (data not shown); minimal log *P* cutoff values of 1.8 ± 0.3 (*38*, *39*), 2.1 ± 0.3 (*37*), and 2.1 ± 0.3 (*41*) as well as a minimal molecular volume cutoff of 250 ± 29 Å^3 (*41*) were calculated. In conclusion, we can say that a combination of structural factors such as size and hydrophobicity play a role in the binding of the aminoadamantane molecules to the TCP locus in either the resting or desensitized state.

Molecular Modeling. For the construction of the AChR molecular model, two approximations were taken into account. One is that the residues were not forced into conformers pointing toward the pore axis. Since the side chains are effectively in a vacuum when they are optimized, rather than a water-filled pore, they tend to fold back on themselves. A second approximation is that the constructed pentameric pore does not have axial symmetry, so there is no corresponding residue exactly across the pore to measure. For this reason, we used the first and third subunits to measure the dimensions of the channel. In this regard, the calculated distances between the centers of the outermost hydrogen atoms for residues at positions M2-2, -6, -9, -13, and -20 were 4.0, 6.65, 10.3, 17.0, and 26.9 Å, respectively. An estimate of the dimensions to the edge of the van der Waals surface can be made by subtracting 1 Å (twice the H atomic radius, 2 × ~0.5 Å). An estimate of the Connoly accessible surface (the surface traced out by the center of a water molecule with a radius of 1.4 Å) can be made by subtracting an additional 2.8 Å from the dimensions of the van der Waals surface. The Connolly surface is considered a good approximation of how close a water or other molecule can be to a protein surface.

With regard to molecular docking, after the short relaxation with restrained molecular dynamics and re-optimization, adamantane remained in an equilibrium position on the pore axis and approximately close to Leu^{251} (position M2-9; see Figure 9). This site coincides, at least partially, with the locus for either TID or barbiturates [between positions M2-9 and M2-13 (*12*)]. The memantine was restrained to Glu^{262} (position M2-20) and remained there. Positively charged amino groups from adamantane derivatives may interact with the carboxylate oxygen of Glu^{262} by H-bonds. In the full receptor, this position would be at the interface of the vestibule formed by the ligand-binding domain and the entrance to the pore (the mouth of the ion channel). The new experimental evidence presented here suggests that the PCP binding site in the resting state may include position M2-20 as well (*18*).

DISCUSSION

Resting Ion Channel. The results of equilibrium binding experiments demonstrate that [^{3}H]TCP, the structural and functional analogue of the hallucinogen and general anes-

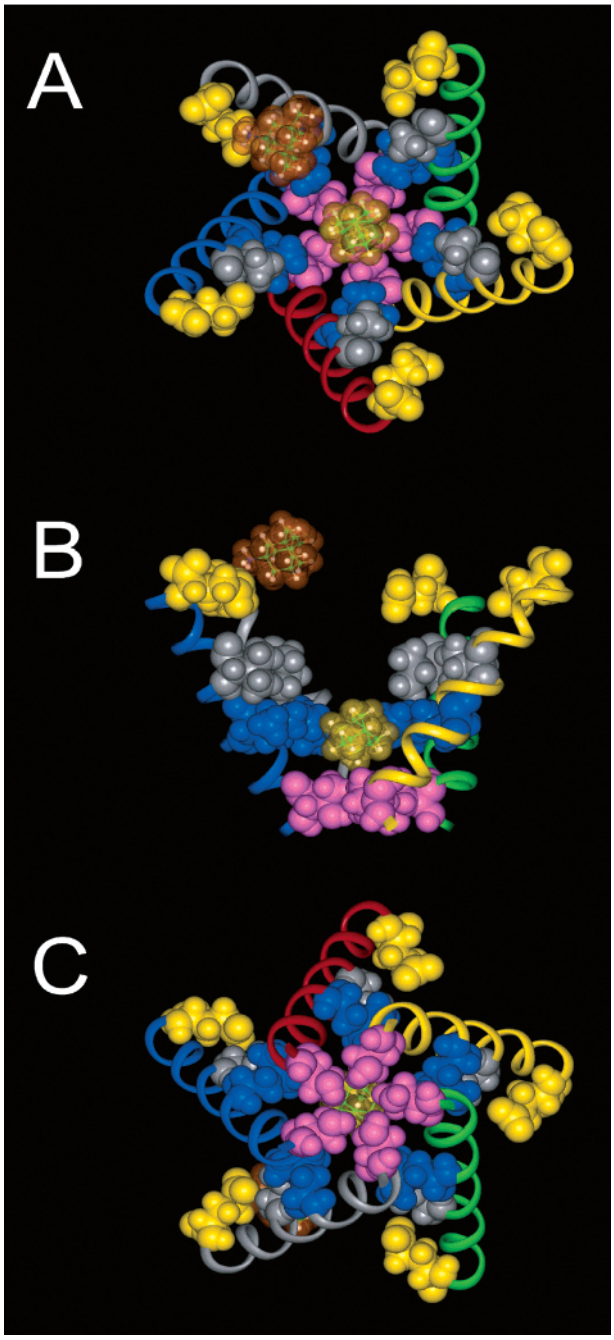

FIGURE 9: Molecular modeling of the AChR ion channel in the resting (closed) state complexed with memantine and adamantane. The model was optimized by obtaining the minimum energy (see Experimental Procedures). The resulting pentameric model of the pore-lining segment of AChR is shown viewed from the synaptic cleft (A), from the plane of the membrane (B), and from the cytoplasmic side of the membrane (C). To visualize better memantine and adamantane molecules within the pore, one M2 segment from the side view is not displayed. A molecule of memantine (transparent orange van der Waals surface with atoms inside rendered as balls and sticks) was inserted above the valine ring (position M2-13, depicted in gray) close to the extracellular ring (position M2-20, depicted in yellow). Positively charged amino groups from adamantane derivatives may interact with αGlu^{262} at position M2-20 via H-bonds. This new evidence suggests that the PCP binding site may include position M2-20 as well (*18*). A neutral adamantane molecule (transparent yellow van der Waals surface with atoms inside rendered as balls and sticks) was placed in the center of mass to find an optimum position (docked) five times. This position is placed close to the conserved leucine ring (position M2-9, depicted in blue). This binding site coincides, at least partially, with the TID and barbiturate locus (*12*). Position M2-2 is depicted in purple.

thetic PCP, binds to a single high-affinity locus in the resting AChR ion channel (Figure 2). The subsequent equilibrium binding and photoaffinity labeling experiments using well-known NCAs as well as a series of adamantane derivatives to probe the structure of the TCP locus in the resting state yielded the following results.

The first set of results indicates that amino group-containing adamantane derivatives specifically displace either [^{3}H]TCP or [^{3}H]tetracaine from its high-affinity site in the resting state in a mutually exclusive manner and with the following rank order: memantine > adamantylethylamine > 1-adamantanamine > 2-adamantanamine > adamantanemethylamine ≫ adamantylpyridinium (Figure 3 and Table 1). Nevertheless, the same derivatives enhance (or not affect) rather than inhibit either [^{14}C]amobarbital binding or [^{125}I]-TID photoincorporation into the resting AChR. All this evidence suggests that the presence of an ammonium group (at pH 7.5, the amine group is 99% positively charged) in the adamantane derivative is required to allow binding to either the TCP or the tetracaine site in the resting channel. One cautionary note, however, is that while our experiments were performed in the absence of agonist and therefore with the resting AChR (a conclusion that is supported by control experiments) it remains possible that the binding of one or more of these adamantane derivatives may induce a conformational change in the AChR.

A second set of results indicates that adamantane (a neutral molecule) displaces either [^{3}H]tetracaine, [^{14}C]amobarbital, or [^{125}I]TID from its respective high-affinity binding site, whereas it enhances [^{3}H]TCP binding in an allosteric manner. In addition, azidoadamantane (a molecule with certain negative charge density conferred by the π electrons on the three nitrogens) fully inhibits [^{3}H]tetracaine but only moderately inhibits [^{3}H]TCP binding. These results suggest that small compounds with no net charge may bind to the tetracaine site in a domain different from the TCP locus (i.e., perhaps the TID or barbiturate locus). This is in agreement with the fact that two small neutral molecules (i.e., TID and barbiturates) also bind to this domain (*12*, *17*). These interpretations are in agreement with the experimental evidence from the Cohen laboratory suggesting that the resting ion channel cannot accommodate two charged molecules at the same time, but one charged and one uncharged molecule (*17*).

A more detailed study on the binding properties of the structurally distinct drugs by thermodynamic (see Table 3) and structural parameters (see Figure 7) indicates the following.

(1) The addition of an amino group (NH_2) at position C1 or C2 of the adamantane molecule allows each adamantanamine isomer to fully bind to either the TCP or tetracaine site (Table 1). For instance, the addition of an ammonium group to the adamantane molecule decreases (in absolute terms) the energy of binding to the tetracaine site by 5.5 kJ/mol (Table 3), an indication of a higher affinity. Since the pK_a for primary amines is between 9.0 and 9.5, the amino group on these molecules should be ∼99% protonated at the experimental pH of 7.5; thus, these compounds would actually be positively charged (H_3N^+). This indicates that the adamantane derivative needs a positive charge for full binding to the TCP locus. This is supported by the fact that 1-adamantanamine and memantine, two positively charged derivatives, inhibit both muscle-type (*23*) and neuronal-type AChRs (*25*, *27*) in a voltage-dependent manner (i.e., more pronounced inhibition at hyperpolarized potentials), and that carboxyl-substituted adamantane analogues are ineffective in interacting with the muscle-type AChR ion channel (*22*). One possibility is that the ammonium group is oriented to the negatively charged amino acid αGlu^{262}, which is located at position M2-20 (see Figure 9).

Nevertheless, we found a contradictory result. Adamantylpyridinium, which also has one permanent positive charge, binds with low affinity to both the TCP and the tetracaine domain (Table 1). A plausible explanation is that the bulky pyridine group prevents the close approach of the positively charged amine to the TCP site by a steric mechanism. In this regard, we can envision the adamantylpyridinium molecule as a neutral but bulky adamantane.

(2) There is a slight increase (in absolute terms) in the binding energy (∼1 kJ/mol; see Table 3) when the position of the ammonium group changes from C1 to C2 in the adamantanamine molecule. This evidence suggests that the position of the ammonium group is not critical for full binding to either the resting or the desensitized ion channel.

(3) The addition of either two methyl groups (two CH_3 groups) or an alkylic chain (=$CHCH_3$) to the 1-adamantanamine molecule as in the case of memantine or adamantylethylamine, respectively, decreases (in absolute terms) the energy of binding by 4.6 or 1.6 kJ/mol, respectively (Table 3). This suggests that hydrophobic interactions increase the affinity for the TCP binding site. This is reflected by the experimental results indicating that *N*,*N*-diethyl-1-adamantanamine has a K_i (determined by competition experiments with [^{3}H]H_{12}-HTX in the resting state) 4-fold lower than that determined for 1-adamantanamine (*21*). However, other parameters such as the increase in molecular size might also be important in explaining the higher affinity observed for either memantine (232 Å^3) or adamantylethylamine (233 Å^3) with respect to 1-adamantanamine (192 Å^3). This idea is supported by previous structure−function relationship studies on the resting AChR, where several 1-adamantanamine analogues with increasing *N*-alkyl chain lengths were used to inhibit [^{3}H]H_{12}-HTX binding with the following rank order (K_is in micromolar) (*21*): *N*-ethyl-1-adamantanamine (*15*) ∼ *N*,*N*-diethyl-1-adamantanamine (*15*) > *N*-methyl-1-adamantanamine (*30*) > *N*-propyl-1-adamantanamine (*40*) ∼ *N*-butyl-1-adamantanamine (*40*) > 1-adamantanamine (*60*).

(4) The elongated distance between the ammonium group and the adamantane ring in adamantanemethylamine caused by the incorporation of a methylene group (CH_2) increases (in absolute terms) the energy of binding to either the TCP (2.3 kJ/mol) or the tetracaine site (1.6 kJ/mol) (Table 3). The observed lower affinity for adamantanemethylamine suggests that the distance between the ammonium group and the adamantane ring is critical for binding to either site. In contrast, the same elongation (CH_2) in the adamantylethylamine molecule decreases (in absolute terms) the energy of binding to each site (Table 3), indicating a higher affinity. One possible explanation for this discrepancy is that the negative effect provoked by the increased distance between the ammonium group and the adamantane ring is partially surmounted by a combination of positive factors such as increased molecular volume and hydrophobicity (as described

in ref *3*) in such a way that adamantylethylamine (log P = 2.19; 233 Å^3) becomes structurally more similar to memantine (log P = 1.97; 232 Å^3).

These structural studies also provided important clues about the size of the NCA binding sites when the ion channel is in the resting state. The comparison between the molecular volumes of either the TCP or the TID locus suggests that the TCP site may accommodate a broader range of molecular volumes (from a minimal volume of 257 ± 64 Å^3 to molecules as large as CrV which has a molecular volume of 461 Å^3) than the TID site, which only can accommodate molecules with volumes no larger than 333 ± 59 Å^3. This is in accord with the idea that there tapering from the extracellular mouth to the cytoplasmic portion of the resting ion channel exists. The molecular modeling of the ion channel in the closed (resting) state depicted in Figure 9 denotes such tapering. For instance, the calculated distances between the van der Waals surface of the outermost hydrogen atoms in the first and third subunits at positions M2-2, -6, -9, -13, and -20 were 3.0, 5.65, 9.3, 16.0, and 25.9 Å, respectively. The diameter of the middle portion of the resting ion channel (presumably at M2-9) was estimated to be ~7 Å as determined by electron microscopy techniques (*47*). This experimental result is a good approximation of our modeling data. Nevertheless, our experimental data and model of the resting ion channel are inconsistent with the recent suggestion that there is an obstruction at the extracellular end of the channel formed by the outer end of the M1 transmembrane segment (*48*).

Desensitized Ion Channel. The same series of adamantane derivatives inhibited [^{3}H]TCP binding to desensitized AChRs with the following rank order (Figure 6A and Table 2): memantine > adamantylethylamine > adamantanemethylamine > 1-adamantanamine > adamantylpyridinium ~ 2-adamantanamine. Practically the same results were obtained by using [^{3}H]ethidium (Figure 6B and Table 2). This is not surprising because PCP displaces ethidium from its high-affinity binding site with a K_i [~0.3 μM (*7*)] similar to its K_d [0.3−0.8 μM (*7*−*9*)]. In turn, a luminal location for the ethidium binding site using photoaffinity labeling was determined (*10*). Thus, we can assume that the binding site for PCP (or TCP) as well as for positively charged adamantane derivatives is located close to the leucine ring (M2-9) within the desensitized ion channel. From these experiments, it is also evident that in this conformational state adamantane inhibits neither [^{3}H]TCP nor [^{3}H]ethidium binding (Figure 6 and Table 2), indicating that this neutral molecule binds to a domain distinct from the TCP (or ethidium) locus in the desensitized state.

Albeit with some quantitative differences, the results from the thermodynamics studies were similar to those with the resting state (see Table 3). Probably the most important distinction between both conformational states is that there is actually a decrease (−1.6 kJ/mol; see Table 3) in the energy of binding to the [^{3}H]TCP site when the distance between the ammonium group and the adamantane ring in 1-adamantanamine is elongated by a methylene group. This result, which is the opposite of that observed in both TCP and tetracaine experiments (Table 3), suggests that the increased distance between the ammonium group and the adamantane ring is a positive structural factor for binding to the TCP site in the desensitized state.

The observed excellent correlation between hydrophobicity (Figure 8A) or molecular volume (Figure 8B) of adamantane derivatives and their K_i values obtained from the [^{3}H]TCP experiments in the desensitized state allowed us to infer both the minimal log P (2.0 ± 0.4) and molecular volume cutoff values (232 ± 22 Å^3) with better accuracy. These minimal cutoff values are similar (2.4 ± 0.5 and 238 ± 53 Å^3, respectively) to those obtained from [^{3}H]ethidium experiments (Figure 8D). In turn, these minimal cutoff values are similar to those obtained in the resting state (2.8 ± 1.0 and 257 ± 64 Å^3, respectively), indicating that the portion of the ion channel corresponding to the TCP locus has practically the same volume and hydrophobicity in either conformational state. However, the fact that there is a more obvious structure−function cutoff in the desensitized than in the resting state suggests that the desensitization process provokes structural constraints in the TCP locus at the level of the middle ion channel.

A distinction in the molecular volume cutoff for the resting (or desensitized) versus the open ion channel is also observed; whereas in the resting and desensitized states cutoffs of 257 (Figure 7B) and 232 Å^3 (Figure 8B,D), respectively, were obtained, larger molecules such as 1-trimethylammonium-5-(1-adamantanemethylammonium)pentane may block the muscle-type AChR ion channel with relatively high affinity [K_d = 13 ± 3 μM at −80 mV (*23*)]. This suggests that the ion channel in the open state is wider than in either the resting or desensitized state.

REFERENCES

1. Arias, H. R. (2000) Localization of agonist and competitive antagonist binding sites on nicotinic acetylcholine receptors, *Neurochem. Int. 36*, 595−645.
2. Corringer, P.-J., Le Novére, N., and Changeux, J.-P. (2000) Nicotinic receptors at the amino acid level, *Annu. Rev. Pharmacol. Toxicol. 40*, 431−458.
3. Arias, H. R. (1998) Binding sites for exogenous and endogenous non-competitive inhibitors of the nicotinic acetylcholine receptor, *Biochim. Biophys. Acta 1376*, 173−220.
4. Arias, H. R. (2001) Thermodynamics of Nicotinic Receptor Interactions, in *Drug-Receptor Thermodynamics: Introduction and Applications* (Raffa, R. B., Ed.) pp 293−358, John Wiley & Sons, New York.
5. Arias, H. R., and Blanton, M. P. (2002) Molecular and physicochemical aspects of local anesthetics acting on nicotinic acetylcholine receptor-containing membranes, *Mini-Rev. Med. Chem. 2*, 385−410.
6. Mosckovitz, R., Haring, R., Gershoni, J. M., Kloog, Y., and Sokolovsky, M. (1987) Localization of azidophencyclidine-binding site on the nicotinic acetylcholine receptor α-subunit, *Biochem. Biophys. Res. Commun. 145*, 810−816.
7. Arias, H. R. (1999) 5-Doxylstearate-induced displacement of phencyclidine from its low-affinity binding sites on the nicotinic acetylcholine receptor, *Arch. Biochem. Biophys. 371*, 89−97.
8. Heidmann, T., Oswald, R. E., and Changeux, J.-P. (1983) Multiple sites of action of noncompetitive blockers on acetylcholine receptor rich membrane fragments from *Torpedo marmorata*, *Biochemistry 22*, 3112−3127.
9. Hann, R. M., Pagán, O. R., Gregory, L., Jácome, T., Rodríguez, A. D., Ferchmin, P. A., Lu, R., and Eterović, V. A. (1998) Characterization of cembranoid interaction with the nicotinic acetylcholine receptor, *J. Pharmacol. Exp. Ther. 287*, 253−260.
10. Pratt, M. B., Pedersen, S. E., and Cohen, J. B. (2000) Identification of the sites of incorporation of [^{3}H]ethidium diazide within the *Torpedo* nicotinic acetylcholine receptor ion channel, *Biochemistry 39*, 11452−11462.
11. Herz, J. M., Johnson, D. A., and Taylor, P. (1989) Distance between the agonist and noncompetitive inhibitor sites on the nicotinic acetylcholine receptor, *J. Biol. Chem. 264*, 12439−12448.

12. Arias, H. R., McCardy, E. A., Gallagher, M. J., and Blanton, M. P. (2001) Interaction of barbiturate analogs with the *Torpedo californica* nicotinic acetylcholine receptor ion channel, *Mol. Pharmacol. 60*, 497−506.
13. Middleton, R. E., Strnad, N. P., and Cohen, J. B. (1999) Photoaffinity labeling the *Torpedo* nicotinic acetylcholine receptor with [^{3}H]tetracaine, a nondesensitizing noncompetitive antagonist, *Mol. Pharmacol. 56*, 290−299.
14. White, B. H., Howard, S., Cohen, S. G., and Cohen, J. B. (1991) The hydrophobic photoreagent 3-(trifluoromethyl)-3-*m*-([^{125}I]-iodophenyl)diazirine is a novel noncompetitive antagonist of the nicotinic acetylcholine receptor, *J. Biol. Chem. 266*, 21595−21607.
15. White, B. H., and Cohen, J. B. (1992) Agonist-induced changes in the structure of the acetylcholine receptor M2 regions revealed by photoincorporation of an uncharged nicotinic noncompetitive antagonist, *J. Biol. Chem. 267*, 15770−15783.
16. Chiara, D. C., Kloczewiak, M. A., Addona, G. H., Yu, J.-A., Cohen, J. B., and Miller, K. W. (2001) Site of resting state inhibition of the nicotinic acetylcholine receptor by a hydrophobic inhibitor, *Biochemistry 40*, 296−304.
17. Gallagher, M. J., Chiara, D. C., and Cohen, J. B. (2001) Interactions between 3-(trifluoromethyl)-3-(m-[^{125}I]iodophenyl)-diazirine and tetracaine, phencyclidine, or histrionicotoxin in the *Torpedo* species nicotinic acetylcholine receptor ion channel, *Mol. Pharmacol. 59*, 1514−1522.
18. Arias, H. R., McCardy, E. A., Bayer, E. Z., Gallagher, M. J., and Blanton, M. P. (2002) Allosterically linked noncompetitive antagonist binding sites in the resting nicotinic acetylcholine receptor ion channel, *Arch. Biochem. Biophys. 403*, 121−131.
19. Gallagher, M. J., and Cohen, J. B. (1999) Identification of amino acids of the *Torpedo* nicotinic acetylcholine receptor contributing for the binding site of the noncompetitive antagonist [^{3}H]tetracaine, *Mol. Pharmacol. 56*, 300−307.
20. Eldefrawi, M. E., Eldefrawi, A. T., Mansour, N. A., Daly, J. W., Witkop, B., and Alburquerque, E. X. (1978) Acetylcholine receptor and ionic channel of *Torpedo* electroplax: binding of perhydro-histrionicotoxin to membrane and solubilized preparations, *Biochemistry 17*, 5474−5484.
21. Warnick, J. E., Maleque, M. A., Bakry, N., Eldefrawi, A. T., and Alburquerque, E. X. (1982) Structure−activity relationship of amantadine. I. Interaction of the N-alkyl analogues with the ionic channel of the nicotinic acetylcholine receptor and electrically excitable membrane, *Mol. Pharmacol. 22*, 82−93.
22. Warnick, J. E., Maleque, M. A., and Alburquerque, E. X. (1984) Interaction of bicyclo-octane analogs of amantadine with ionic channels of the nicotinic acetylcholine receptor and electrically excitable membrane, *J. Pharmacol. Exp. Ther. 228*, 73−79.
23. Antonov, S. M., Johnson, J. W., Lukomskaya, N. Y., Potapyeva, N. N., Gmiro, V. E., and Magazanik, L. G. (1995) Novel adamantane derivatives act as blockers of open ligand-gated channels and as anticonvulsants, *Mol. Pharmacol. 47*, 558−567.
24. McKay, D. B., and Trent-Sanchez, P. (1990) Effect of non-competitive nicotinic receptor blockers on catecholamine release from cultured adrenal chromaffin cells, *Pharmacology 40*, 224−230.
25. Matsubayashi, H., Swanson, K. L., and Alburquerque, A. X. (1997) Amantadine inhibits nicotinic acetylcholine receptor function in hippocampal neurons, *J. Pharmacol. Exp. Ther. 281*, 834−844.
26. Alburquerque, E. X., Pereira, E. F., Braga, M. F., Matsubayashi, H., and Alkondon, M. (1998) Neuronal nicotinic receptors modulate synaptic function in the hippocampus and are sensitive to blockade by the convulsant strychnine and by the anti-Parkinson drug amantadine, *Toxicol. Lett. 102−103*, 211−218.
27. Buisson, B., and Bertrand, D. (1998) Open-channel blockers at the human $\alpha 4\beta 2$ neuronal nicotinic acetylcholine receptor, *Mol. Pharmacol. 53*, 555−563.
28. Oliver, D., Ludwig, J., Reisinger, E., Zoellner, W., Ruppersberg, J. P., and Fakler, B. (2001) Memantine inhibits efferent cholinergic transmission in the cochlea by blocking nicotinic acetylcholine receptors of outer hair cells, *Mol. Pharmacol. 60*, 183−189.
29. Katz, E. J., Cortes, V. I., Eldefrawi, M. E., and Eldefrawi, A. T. (1997) Chlorpyrifos, parathion, and their oxons bind to and desensitize a nicotinic acetylcholine receptor: relevance to their toxicities, *Toxicol. Appl. Pharmacol. 146*, 227−236.
30. Pagán, O. R., Eterović, V. A., García, M., Vergne, D., Basilio, C. M., Rodríguez, A. D., and Hann, R. M. (2001) Cembranoid and long-chain alkanol sites on the nicotinic acetylcholine receptor and their allosteric interaction, *Biochemistry 40*, 11121−11130.
31. Pedersen, S. E., Dreyer, E. B., and Cohen, J. B. (1986) Location of ligand binding sites on the nicotinic acetylcholine receptor α subunit, *J. Biol. Chem. 261*, 13735−13743.
32. Moore, M. A., and McCarthy, M. P. (1995) Snake venom toxins, unlike smaller antagonists, appear to stabilize a resting state conformation of the nicotinic acetylcholine receptor, *Biochim. Biophys. Acta 1235*, 336−342.
33. Scatchard, G. (1949) The attraction of proteins for small molecules and ions, *Ann. N.Y. Acad. Sci. 51*, 660−672.
34. Blanton, M. P., McCardy, E. A., and Gallagher, M. J. (2000) Examining the noncompetitive antagonist-binding site in the ion channel of the nicotinic acetylcholine receptor in the resting state, *J. Biol. Chem. 275*, 3469−3478.
35. Cheng, Y. C., and Prusoff, W. H. (1973) Relationship between the inhibition constant (K_i) and the concentration of inhibitor which causes 50% inhibition (IC_{50}) of an enzymatic reaction, *Biochem. Pharmacol. 22*, 3099−3108.
36. Hansch, C., Bjorkroth, J. P., and Leo, A. (1987) Hydrophobicity and central nervous system agents: on the principle of minimal hydrophobicity in drug design, *J. Pharm. Sci. 76*, 663−687.
37. Ghose, A. K., Pritchett, A., and Crippen, G. M. (1988) Atomic physicochemical parameters for three-dimensional-structure-directed quantitative structure−activity relationships. 3. Modeling hydrophobic interactions, *J. Comput. Chem. 9*, 80−90.
38. Kantola, A., Villar, H. O., and Loew, G. H. (1991) Atom based parametrization for a conformationally dependent hydrophobic index, *J. Comput. Chem. 12*, 681−689.
39. Alkorta, I., and Villar, H. O. (1992) Quantum mechanical parametrization of a conformationally dependent hydrophobic index, *Int. J. Quantum Chem. 44*, 203−218.
40. Dodd, L. R., and Theodorou, D. N. (1991) Analytical treatment of the volume and surface area of molecules formed by an arbitrary collection of unequal spheres intersected by planes, *Mol. Phys. 72*, 1313−1345.
41. Dewar, M. J. S., Zoebisch, E. G., Healy, E. F., and Stewart, J. J. P. (1985) AM1: a new general purpose quantum mechanical molecular model, *J. Am. Chem. Soc. 107*, 3902−3909.
42. Chang, G., Spencer, R. H., Lee, A. T., Barclay, M. T., and Rees, D. C. (1998) Structure of the MscL homolog from *Mycobacterium tuberculosis*: a gated mechanosensitive ion channel, *Science 282*, 2220−2226.
43. Bertaccini, E., and Trudell, J. R. (2001) Molecular modeling of ligand-gated ion channels: progress and challenges, *Int. Rev. Neurobiol. 48*, 141−166.
44. Lurtz, M. M., and Pedersen, S. E. (1999) Aminotriarylmethane dyes are high-affinity noncompetitive antagonists of the nicotinic acetylcholine receptor, *Mol. Pharmacol. 55*, 159−167.
45. Arias, H. R., McCardy, E. A., and Blanton, M. P. (2001) Characterization of the dizocilpine binding site on the nicotinic acetylcholine receptor, *Mol. Pharmacol. 59*, 1051−1060.
46. Ryan, S. E., Blanton, M. P., and Baenziger, J. E. (2001) A conformational intermediate between the resting and the desensitized states of the nicotinic acetylcholine receptor, *J. Biol. Chem. 276*, 4796−4803.
47. Unwin, N. (2000) The Croonian Lecture 2000. Nicotinic acetylcholine receptor and the structural basis of fast synaptic transmission, *Philos. Trans. R. Soc. London, Ser. B 355*, 1813−1829.
48. Yu, Y., Shi, L., and Karlin, A. (2003) Structural effects of quinacrine binding in the open channel of the acetylcholine receptor, *Proc. Natl. Acad. Sci. U.S.A. 100*, 3907−3912.